Available online at www.sciencedirect.com

ScienceDirect

Procedia Structural Integrity 2 (2016) 2849–2856

Structural Integrity Procedia

www.elsevier.com/locate/procedia

21st European Conference on Fracture, ECF21, 20-24 June 2016, Catania, Italy

Study of the influence of the oxide and concrete parameters on the results of accelerated corrosion tests

Beatriz Sanz[a,*], Jaime Planas[a], José M. Sancho[b]

[a] *Universidad Politécnica de Madrid, ETSI Caminos, Canales y Puertos, Profesor Aranguren 3, 28040 Madrid, Spain*
[b] *Universidad Politécnica de Madrid, ETS de Arquitectura, Avda. Juan de Herrera 3, 28040 Madrid, Spain*

Abstract

In this work, a numerical study is presented to analyze the influence of the oxide and concrete parameters on the results of cracking induced by corrosion. The results of two-dimensional models of prisms reinforced with a bar and prisms reinforced with a tube are compared. For the simulations, a model has been used that reproduces the cohesive fracture of concrete and the expansive behavior of the oxide. As a reference, the results of accelerated corrosion tests of prisms reinforced with a tube equipped with special instruments to measure the deformation of the tube are provided, with good agreement. Differences have been observed between the models with a bar and models with a tube in the sensitivity of the curves of results to variations in the model parameters, which have been crucial for indirect determination of the oxide parameters, as discussed in the paper.

Peer-review under responsibility of the Scientific Committee of ECF21.

Keywords: Finite element modeling, cohesive crack, reinforced concrete, accelerated corrosion, fracture mechanics

1. Introduction

Cracking of the cover might occur when structures suffer corrosion of the reinforcement, due to the generation of an oxide layer that occupies a volume greater than that of steel (Andrade et al., 1993; Tuutti, 1982). To simulate that effect and to predict the degree of safety of affected structures, it is essential to model the fracture behavior of concrete and the oxide expansion. For the concrete, models and experimental methods are available to describe its cracking and to determine the parameters defining it, as the method proposed by Planas et al. (2007), which combines the results of stable three point bending tests on notched beams and brazilian tests to calculate a bilinear softening curve, following the standard cohesive model introduced by Hillerborg et al. (1976). However, for the oxide layer direct experimental characterization is very difficult, since oxide evolves with the conditions of the medium (Andrade et al., 1996), and indirect analysis arises as the main option to obtain information from the results of experiments and models.

For achieving reliable conclusions from indirect analyses, one of the key aspects is that the measurements used as a reference from experiments are sensitive enough to variations in the model parameters being determined; otherwise the parameters are calculated with a high error. For example, the typical measurement of crack width is barely affected by

* Corresponding author. Tel.: +34-91-336-5244 ; fax: +34-91-336-6680.
E-mail address: beatriz.sanz@upm.es

Peer review under responsibility of the Scientific Committee of ECF21.
10.1016/j.prostr.2016.06.356

high variations in the oxide stiffnesses, and, thus, only the expansion factor of the oxide can be inferred from that with enough precision, as will be discussed in the paper. Another important aspect is that the models reproduce accurately the conditions in the experiments; otherwise, unrealistic results are obtained.

Attending to those conditions, a study was presented by Sanz et al. (2015) using as specimens concrete prisms reinforced with a smooth steel tube. Accelerated corrosion tests were performed with clear boundary conditions reproducible in simulations with two-dimensional models of the specimens. For the simulations, a model was used that combines finite elements with an embedded crack to reproduce the cohesive fracture of concrete (Sancho et al., 2007a), and expansive joint elements to reproduce the oxide behavior (Sanz et al., 2013). During the tests, information about the inner deformation of the tube was recorded, which, in addition to the crack opening and the crack pattern at the end of the tests, allowed to calculate approximate values for the oxide parameters (Sanz et al., 2015; Sanz, 2014).

In this work, a numerical study is presented to compare the results of simulations using models of prisms reinforced with a bar and of prisms reinforced with a tube, and the advantages of using a tube instead of a bar in the determination of the oxide parameters are discussed. Then the influence of the oxide and concrete parameters on the curves of results is analyzed, with further support of the results presented in Sanz et al. (2015).

Nomenclature

f_t	tensile strength of the concrete
G_{F_1}	fracture energy of the linear softening curve
k_n^0	cutoff of the normal stiffness k_n of the expansive joint element
k_t^0	cutoff of the shear stiffness k_t of the expansive joint element
x	corrosion depth, i.e., amount of steel transformed into oxide
w_1	horizontal intercept of the linear softening curve
α'	adaption factor of the crack
β	expansion factor of the expansive joint element
η	directionality factor of the expansive joint element

2. Numerical study

2.1. Numerical model

Simulations of accelerated corrosion have been carried out using the model presented in Sanz et al. (2013), whose main characteristics are briefly explained next for completeness of the text.

Fracture of concrete is assumed to follow the standard cohesive model (Hillerborg et al., 1976), in which a crack transmits stresses following a *softening curve*, as sketched in Fig. 1(a). To simplify the calculations, a linear approach of the softening curve was used in the numerical study, in which only initiation of cracking is sought for comparative purposes, while for definitive simulations of the tests, in which wide crack openings are reached, a bilinear curve was used. The cohesive behavior is implemented in elements with an *embedded adaptable crack* (Sancho et al., 2007a,b), within the finite element framework COFE (*Continuum Oriented Finite Element*). Those are constant strain triangles, in which the crack is a strong discontinuity in the element that follows a central force model and can reorient according to the stress field until a given threshold value w_{th} is reached, which is calculated as $w_{th} = \alpha' w_1$, where α' is the adaption factor of the crack, and w_1 the horizontal intercept of the linear softening curve, defined in Fig. 1(a).

The oxide behavior is implemented in *expansive joint elements*, which incorporate its expansion and its mechanical behavior (Sanz et al., 2013). The increment of volume is reproduced as a free expansion perpendicular to the element, see Fig. 1(b), calculated as βx, where β is the expansion factor of the oxide, and x is the corrosion depth or amount of steel that is transformed into oxide. To simulate a fluid-like behavior, debonding and separation effects are implemented, by means of a small shear stiffness k_t and a directionality factor η that diminishes the normal stiffness k_n for tensile stress. To avoid re-meshing, a simplification is introduced by keeping constant the steel section during the calculations; thus, mechanical equivalence of the real and simulated systems is imposed, from which fictitious stiffnesses

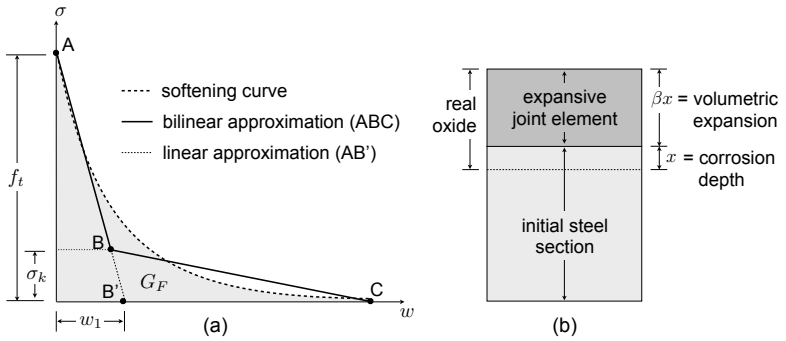

Fig. 1. Softening curve of concrete, bilinear and linear approaches, and parameters defining them (a), where f_t is the tensile strength, G_F the fracture energy, w_1 the horizontal intercept of the linear curve and σ_k the stress of the kink point; and sketch of the expansive joint element (b).

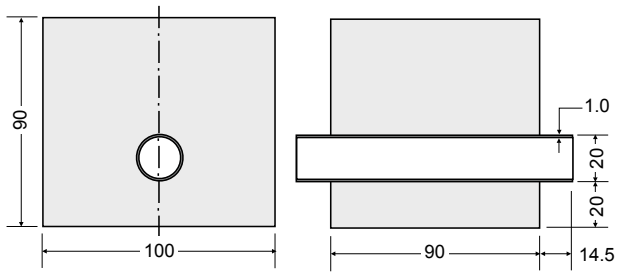

Fig. 2. Geometry of the specimens, with dimensions in mm.

of the element are calculated that turn out to be inversely proportional to the corrosion depth x, and numerical cutoffs k_n^0 and k_t^0 are set for a small corrosion depth x_0. See Sanz et al. (2013) for the formulation of the elements.

2.2. Specimens and parameters in the simulations

In the numerical study, the tests reported in Sanz et al. (2015) have been taken as a reference. In those, the specimens were concrete prisms reinforced with a smooth steel tube, as sketched in Fig. 2, which were designed to obtain a single main crack at the cover. They were fabricated with concrete containing chlorides, to produce depassivation of the steel; hence, this study does not cover the income of aggressive substances and focuses only on the propagation of corrosion.

Two-dimensional models of those specimens have been used in the simulations. Models of prisms with the same geometry but reinforced with a bar have been also used for comparative purposes. In both, the mesh was generated with the free-domain program Gmsh (Geuzaine and Remacle, 2009), with the type of elements indicated in Fig. 3. The number of elements at the oxide interface was 32 in models with a bar and 64 in models with a tube, as set in previous studies (Sanz et al., 2013, 2015), and the size of the elements at the outer boundary was five times greater.

The calculations were driven by the corrosion depth x, from which the free radial expansion βx was computed at each step. A total depth of 20 μm was imposed at 40 steps, which was enough to obtain a stable crack pattern.

Table 1 shows the properties of the materials. For the steel, elastic behavior with standard values was assumed. For the concrete, its fracture parameters were determined in experiments (Sanz et al., 2015), following the method proposed by Planas et al. (2007). Finally, for the oxide, the values reported in Sanz et al. (2013) were used as a reference, which are based on a fluid-like behavior, with an expansion factor $\beta = 1.0$ as proposed by Molina et al. (1993), and almost perfect free debonding and separation. To test the sensitivity of the results to large variations of the constitutive parameters of the expansive joint element, simulations were run within the ranges of values indicated in Table 2, while keeping the remaining parameters with the base values of Table 1.

During the tests, the prisms were corroded using the impressed current technique (Andrade et al., 1993; El Maaddawy and Soudki, 2003). In the simulations, the experimental measurements were reproduced, recording the displace-

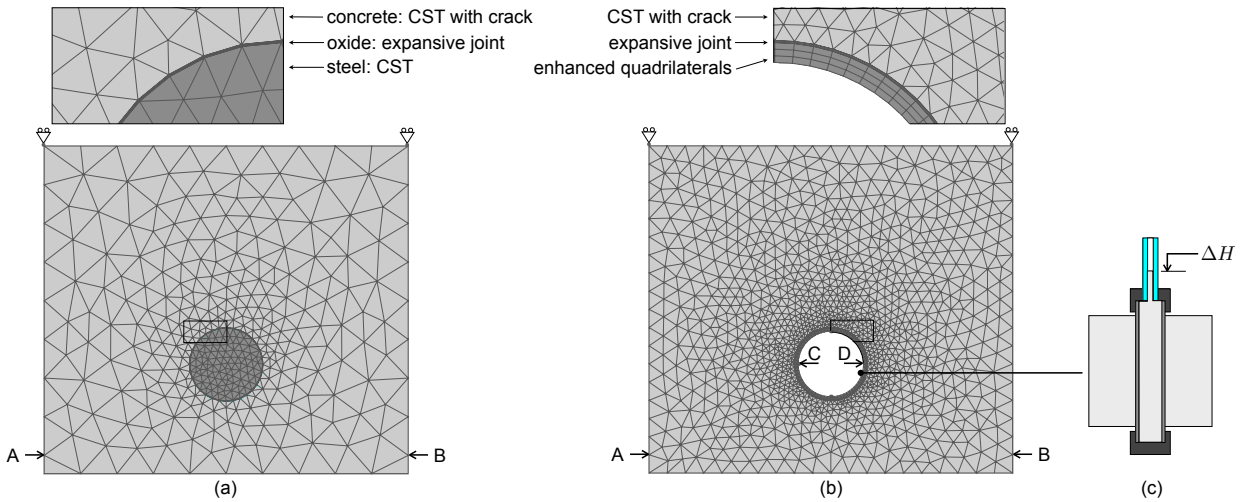

Fig. 3. Mesh of models of prisms reinforced with a bar (a) and prisms reinforced with a tube (b), where CST are Constant Strain Triangles, and measurements: main CMOD (displacement between A and B), variation of inner diameter between C and D, and variation of capillary height (c).

Table 1. Base parameters of the materials, where E is the elastic modulus, ν Poisson's ratio, f_t the tensile strength, G_{F_1} the fracture energy below the linear softening curve, w_1 the horizontal intercept of the linear curve with the abscissas axis, α' the adaption factor of the crack, β the volumetric expansion factor, x_0 the cutoff corrosion depth, k_n^0 and k_t^0 the cutoff normal and shear stiffnesses and η the reduction factor of the tensile stiffness.

Material	E (GPa)	ν	f_t (MPa)	G_{F_1} (N/mm)	w_1 (mm)	α'	β	x_0 (mm)	k_n^0 (N/mm^3)	k_t^0 (N/mm^3)	η
Steel	200	0.3	—	—	—	—	—	—	—	—	—
Concrete	36.1	0.2	2.78	0.0597	0.0430	0.2	—	—	—	—	
Oxide	—	—	—	—	—	—	1.0	1.0×10^{-3}	1.0×10^{6}	1.0×10^{-14}	1.0×10^{-11}

Table 2. Range of parameters in the numerical study, where k_n^0 and k_t^0 are the cutoff normal and shear stiffnesses, η the reduction factor of the tensile stiffness, β the expansion factor and G_{F_1} the fracture energy below the linear softening curve.

Parameter	Values in the parametric study
k_n (N/mm^3)	1.0×10^{3}, 1.0×10^{4}, 1.0×10^{5}, 1.0×10^{6}, 1.0×10^{7}, 1.0×10^{8}
k_t (N/mm^3)	1.0×10^{-100}, 1.0×10^{-14}, 1.0×10^{0}, 1.0×10^{1}, 1.0×10^{2}, 1.0×10^{3}, 1.0×10^{4}, 1.0×10^{5}, 1.0×10^{6}
η_t	1.0×10^{-100}, 1.0×10^{-11}, 1.0×10^{-6}, 1.0×10^{-3}, 1.0×10^{-2}, 1.0×10^{-1}, 1.0×10^{0}
β	1.0, 1.25, 1.5, 1.75, 2.0
G_{F_1} (N/mm)	0.030, 0.060, 0.120

ment at the corresponding nodes: the *main CMOD*, which is the width of the main crack at the middle section of the specimen between points A and B defined in Fig. 3, the variation of inner diameter ΔD, measured with special extensometers at the diameter perpendicular to the expected main crack between points C and D, and the variation of capillary height ΔH, which is related with the variation of inner volume of the tube, and is measured as the variation of liquid within a capillary tube in a sealed circuit that connects it with the steel tube, as sketched in Fig. 3(c). See Sanz et al. (2015) for the design of the instruments. In the models with a bar, only the main CMOD was simulated.

3. Results and discussion

3.1. Results of models of prisms reinforced with a bar

Figure 4 shows the results of the numerical study for models of prisms reinforced with a bar. The effect of the

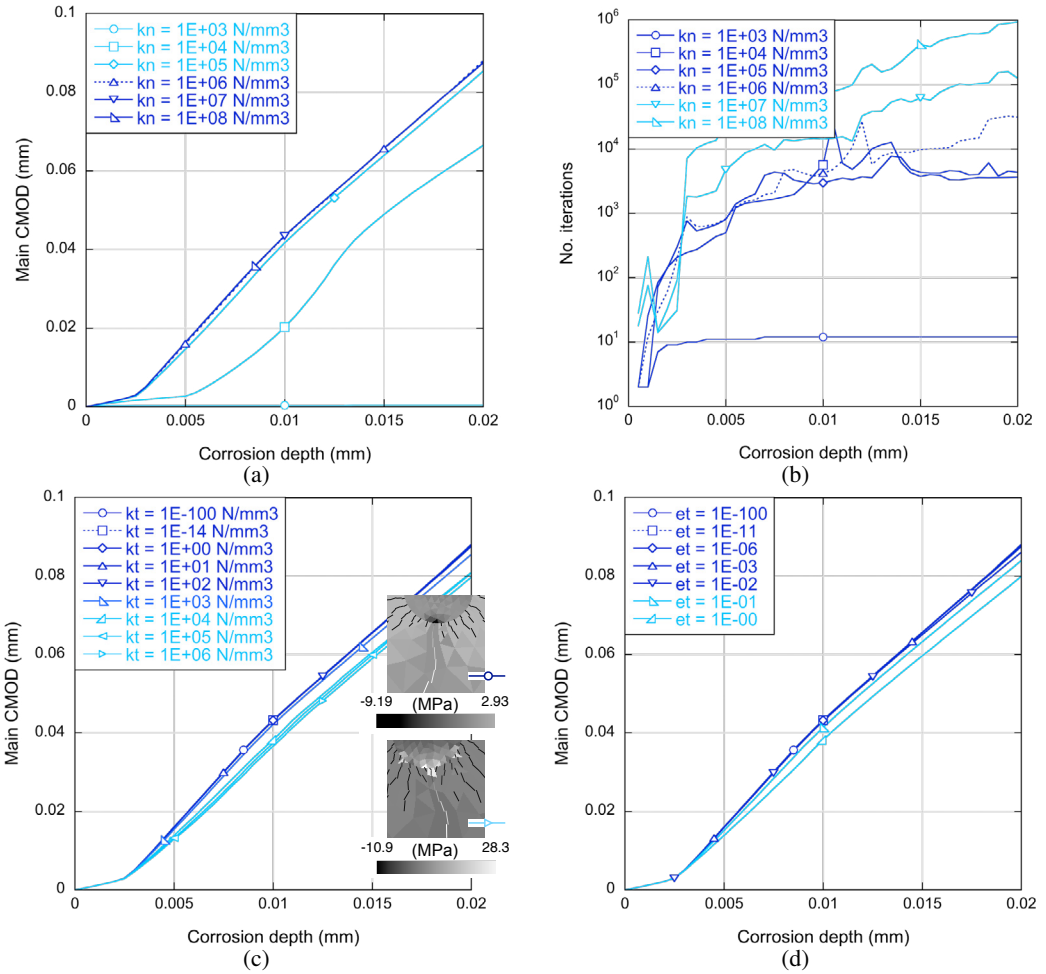

Fig. 4. Parametric study in models of prisms reinforced with a bar: effect of the normal stiffness k_n^0 on the main CMOD (a) and on the number of iterations (b), and effect on the main CMOD of the shear stiffness k_t^0 (c) and of the directionality factor η (d).

normal stiffness k_n^0 on the curves of crack width, Fig. 4(a), was negligible for $k_n^0 \geq 10^6$ N/mm^3, although the number of iterations, Fig. 4(b), increased. It is noticeable that for $k_n^0 = 10^3$ N/mm^3 the oxide was too flexible and no cracking occurred. Regarding the shear stiffness k_t^0, Fig. 4(c), it barely affected the main CMOD, specially for $k_t^0 \leq 10^3$ N/mm^3. However, for values greater than that, the cracks were clamped at their root and stress concentration points appeared, as manifested by the white triangle in the detail of stress map around the main crack shown in the right part of the figure, which motivated introducing the debonding ability of the model. The effect of the directionality factor η, Fig. 4(d), was as that of the shear stiffness, including clamping of cracks, although less pronounced.

3.2. Results of models of prisms reinforced with a tube

Figure 5 shows the results of the numerical study for prisms reinforced with a tube. The effect of the normal stiffness k_n^0, Fig. 5(a), is as that observed in prisms with a bar. Thus, $k_n^0 = 10^6$ N/mm^3 was selected as the best value for that, which is coherent with a behavior as that of water, with the minimum number of iterations. Regarding the shear stiffness k_t^0, Fig. 5(b), it affected the main CMOD as in prisms with a bar but more pronouncedly; however, in prisms with a tube it affected drastically the number of cracks, as shown in the details on the right, which was not manifested in prisms with a bar. Finally, the effect of the directionality factor η, Fig. 5(c), was as that of prisms with a bar, so this factor was kept as in reference simulations, which is in coherent with the hypothesis of a fluid-like behavior.

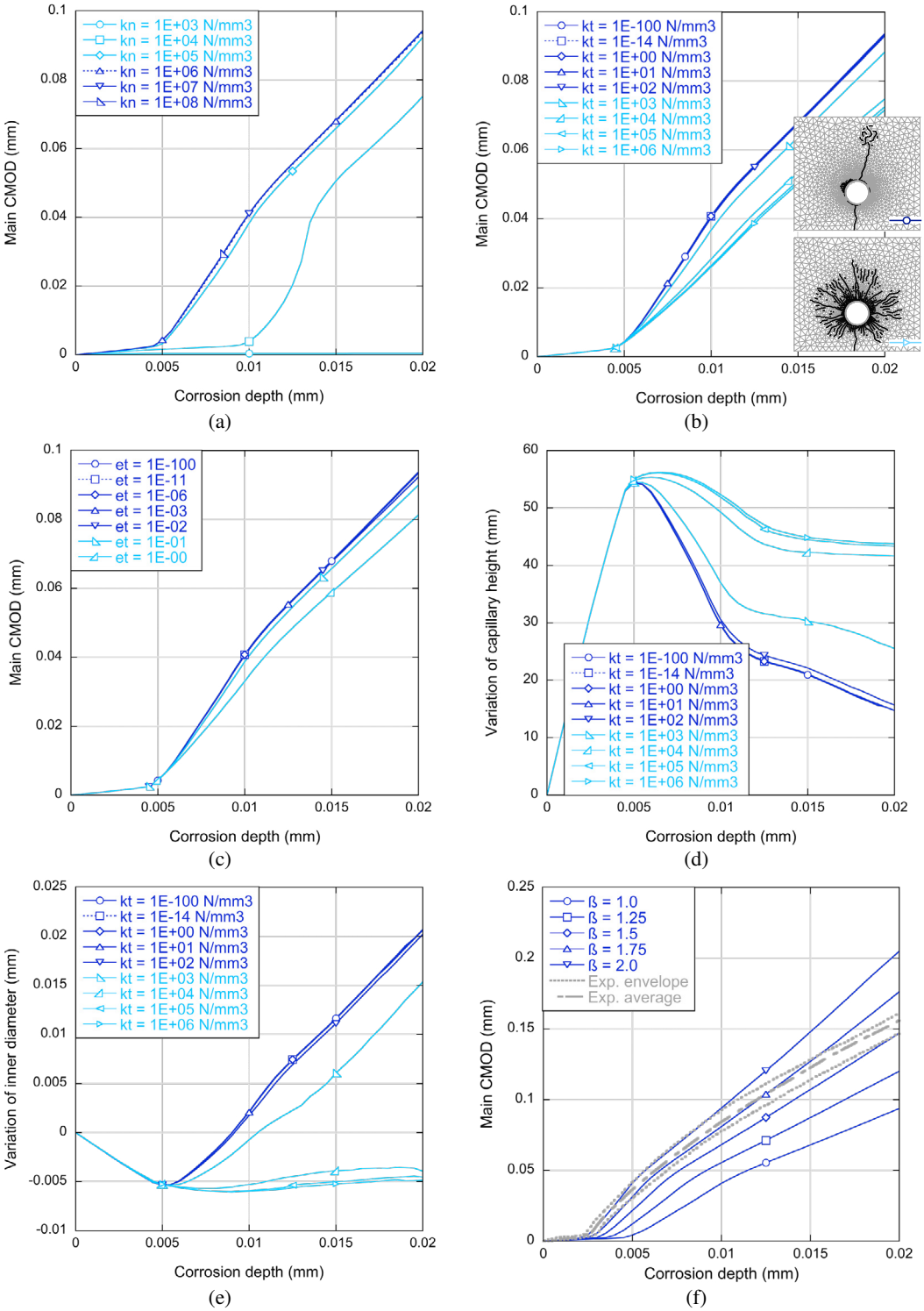

Fig. 5. Parametric study in models of prisms reinforced with a tube: effect on the main CMOD of the normal stiffness k_n^0 (a), the shear stiffness k_t^0 (b) and the directionality factor η (c), effect of the shear stiffness k_t^0 on the curves of variation of capillary height (d) and inner diameter (e) and effect of the expansion factor on the main CMOD (f).

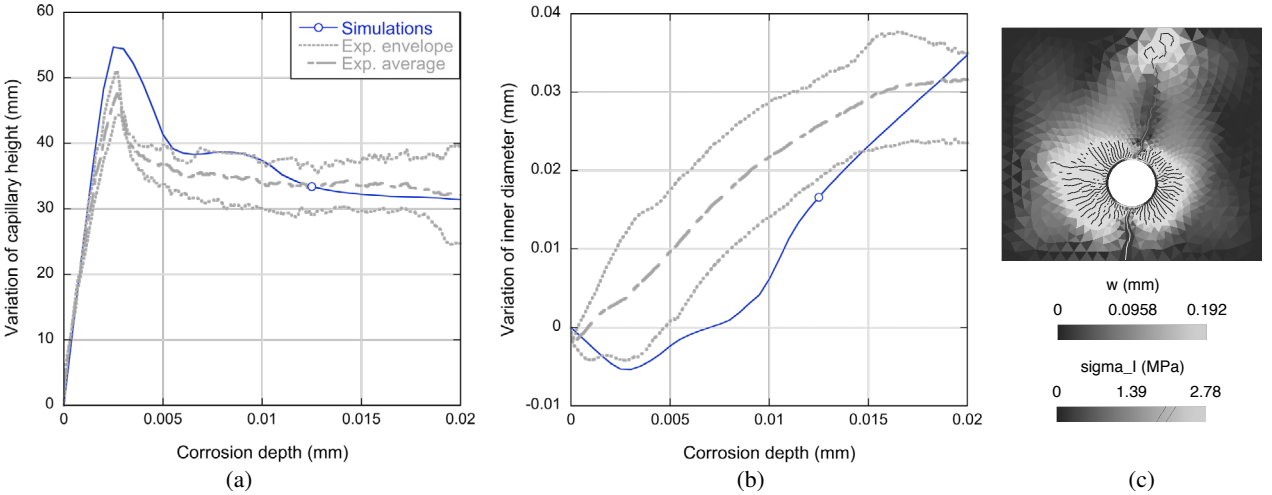

Fig. 6. Results of simulations of accelerated corrosion tests and experimental results: curves of variation of capillary height (a) and of variation of inner diameter (b), and simulated stress map and crack pattern for a corrosion depth of 20 μm (c). See Fig. 6(d) for the results of main CMOD.

From the foregoing results, it is concluded that the main CMOD of prisms with a tube is more sensitive to variations in the oxide parameters than that of prisms with a bar. Besides, prisms with a tube provided extra information about the variation of inner volume –measured through the capillary height– and inner diameter of the tube, which result to be much more sensitive to variations in the oxide parameters than the main CMOD. As an example, Figs. 5(d) and (e) display the effect of the shear stiffness k_t^0 on the curves of capillary height and inner diameter.

Then the best values for the model parameters were determined, taking as a reference the experimental results obtained in Sanz et al. (2015). Firstly the expansion factor β, which scales the curves of results on the corrosion-depth axis as shown in Fig. 5(f), was modified until the numerical curves fitted the experimental ones, finding that the best value was $\beta = 2.0$. Next, the shear stiffness k_t^0 was adjusted, using the new value of β and bilinear softening with fracture energy $G_F = 0.107$ N/mm and stress at the kink point $\sigma_k = 0.322$ MPa, finding that $k_t^0 = 1000\text{N/mm}^3$ was the best value for that. Figs. 6(a) and (b) display the resulting curves of variation of capillary height and inner diameter, showing a good agreement with the experimental results. Finally, it was assessed that the crack pattern at the end of the simulations, Fig. 6(c), resembled the experimental one, which consisted of a main crack and between four and eight secondary cracks surrounding the reinforcement, as observed in slices of the specimens impregnated with fluorescent resin (Sanz et al., 2013).

For completeness of this study, the effect of the fracture energy of the linear curve G_{F_1} is shown in Fig. 7. As observed for the oxide parameters, the effect was greater on the curves of variation of capillary height, Fig. 7(a), and inner diameter than on the curves of main CMOD Fig. 7(b).

4. Conclusions

A numerical study has been carried out to investigate the influence of the oxide parameters on the results of accelerated corrosion of reinforced concrete structures. For that, two-dimensional models of concrete prisms reinforced with a bar and prisms reinforced with a tube have been used. A model has been applied that reproduces the cohesive fracture of concrete and the expansive behavior of the oxide. The results have been compared with those of accelerated corrosion tests designed with conditions reproduceable in two-dimensional models.

From the study, it has been observed that the measurement of main CMOD is more affected by variations in the oxide parameters in models with a tube than in models with a bar. Besides, the curves of variation of inner diameter and capillary height recorded in prisms with a tube are much more sensitive than the main CMOD to the oxide and concrete parameters. Thus, using prisms reinforced with a tube has been crucial in this research to obtain the best values for the constitutive parameters of the oxide, which could be applied in further studies.

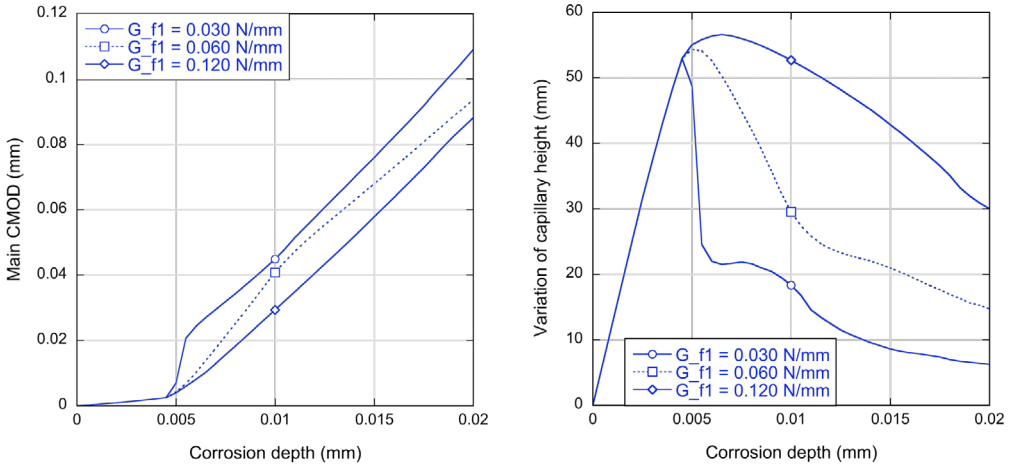

Fig. 7. Effect of the fracture energy of the linear softening curve G_{F_1} on the curves of main CMOD (a) and capillary height (b).

Acknowledgements

The authors gratefully acknowledge the *Secretaría de Estado de Investigación, Desarrollo e Innovación* of the Spanish *Ministerio de Economía y Competitividad* for providing financial support for this work under the project BIA2014-54916-R.

References

Andrade, C., Alonso, C., Rodríguez, J., García, M., 1996. Cover cracking and amount of rebar corrosion: importance of the current applied in accelerated tests, in: Dhir, R.K., Jones, M.R. (Eds.), Concrete in the Service of Mankind, Concrete repair, rehabilitation and protection, E&FN Spon, London, UK. pp. 263–273.

Andrade, C., Alonso, M., Molina, F., 1993. Cover cracking as a function of bar corrosion: Part i - experimental test. Materials and Structures 26, 453–464. doi:10.1007/BF02472805.

El Maaddawy, T., Soudki, K., 2003. Effectiveness of impressed current technique to simulate corrosion of steel reinforcement in concrete. Journal of Materials in Civil Engineering 15, 41–47. doi:10.1061/(ASCE)0899-1561(2003)15:1(41).

Geuzaine, C., Remacle, J.F., 2009. Gmsh: a three-dimensional finite element mesh generator with built-in pre- and post-processing facilities. International Journal for Numerical Methods in Engineering 79, 1309–1331. doi:10.1002/nme.2579.

Hillerborg, A., Modéer, M., Petersson, P., 1976. Analysis of crack formation and crack growth in concrete by means of fracture mechanics and fracture elements. Cement and concrete research 6, 773–781. doi:10.1016/0008-8846(76)90007-7.

Molina, F., Alonso, M., Andrade, C., 1993. Cover cracking as a function of bar corrosion: Part ii - numerical model. Materials and Structures 26, 532–548. doi:10.1007/BF02472864.

Planas, J., Guinea, G.V., Galvez, J.C., Sanz, B., Fathy, A.M., 2007. Report 39: Experimental Determination of the Stress-Crack Opening Curve for Concrete in Tension - Final report of RILEM Technical Committee TC 187-SOC. RILEM Publications SARL. chapter 3. Indirect tests for stress-crack opening curve. pp. 13–29.

Sancho, J.M., Planas, J., Cendon, D.A., Reyes, E., Galvez, J.C., 2007a. An embedded cohesive crack model for finite element analysis of concrete fracture. Engineering Fracture Mechanics 74, 75–86. doi:10.1016/j.engfracmech.2006.01.015.

Sancho, J.M., Planas, J., Fathy, A.M., Gálvez, J.C., Cendón, D.A., 2007b. Three-dimensional simulation of concrete fracture using embedded crack elements without enforcing crack path continuity. International Journal for Numerical and Analytical Methods in Geomechanics 31, 173–187. doi:10.1002/nag.540.

Sanz, B., 2014. Experimental and numerical study of cracking of concrete due to reinforcement corrosion. Ph.D. thesis. Universidad Politécnica de Madrid.

Sanz, B., Planas, J., Sancho, J., 2015. A closer look to the mechanical behavior of the oxide layer in concrete reinforcement corrosion. International Journal of Solids and Structures 62, 256 – 268. doi:10.1016/j.ijsolstr.2015.02.040.

Sanz, B., Planas, J., Sancho, J.M., 2013. An experimental and numerical study of the pattern of cracking of concrete due to steel reinforcement corrosion. Engineering Fracture Mechanics 114, 26–41. doi:10.1016/j.engfracmech.2013.10.013.

Tuutti, K., 1982. Corrosion of steel in concrete. volume 4.82 of *CBI Forskning 82:4*. Swedish Cement and Concrete Research Institute.